An Antirotation Wireless Power Transfer System With a Flexible Magnetic Coupler for Autonomous Underwater Vehicles

Ben Zhang, *Graduate Student Member, IEEE*, C. Q. Jiang, *Senior Member, IEEE*, Fengshuo Yang, Chen Chen, Yong Lu, and Jiayu Zhou

***Abstract*—Combining wireless power transfer (WPT) technology with an underwater inclusive charging platform is an effective method to solve the problem of energy replenishment for autonomous underwater vehicles (AUVs). To ensure a stable charging state of the AUV at arbitrary positions, an antirotation flexible magnetic coupler (FMC) is proposed in this article. The transmitter structure can follow the retractable cage changes of the charging platform. Through the optimization analysis, the FMC, composed of a single-layer transmitter coil and a double-layer receiver coil and rotated 45° between the two layers of receiver coils, has excellent antirotation capability under 360° rotations. Moreover, the magnetic field of the FMC is evenly distributed and concentrated between the magnetic cores of the transmitter and receiver, causing little effect on the equipment inside the AUV. To address the coupling parameter variations due to AUV rotation and the transmitter contraction during FMC operation, soft switching of the WPT system is achieved by pulse density modulation and slight detuning of the resonator. An experimental prototype was established to verify the antirotation characteristics of the FMC as well as the soft-switching attributes of the system, and the experimental results matched well with the simulations.**

***Index Terms*—Antirotation, autonomous underwater vehicles (AUVs), flexible magnetic coupler (FMC), pulse density modulation (PDM), wireless power transfer (WPT).**

I. Introduction

With the advancement of science and technology, there has been an acceleration in the exploration of the oceanic domain. Autonomous underwater vehicles (AUVs), as intelligent devices capable of independently executing underwater tasks, play a vital role in various fields, such as marine exploration, environmental monitoring, and military applications [1]. AUVs rely on the energy stored in their batteries, which limits their operational depth and endurance [2]. The traditional methods of energy replenishment include retrieving the AUVs to the surface for battery replacement or employing a wet-plug interface for wired charging underwater. These methods have drawbacks, including poor reliability, safety, and autonomy.

Under the situation mentioned above, wireless power transfer (WPT) technology has emerged, offering an innovative solution [3], [4]. In contrast to traditional wired charging, WPT utilizes electromagnetic fields to transmit energy, eliminating the need for physical connections and enhancing safety and reliability [5]. Particularly in underwater environments, WPT technology can significantly improve operational flexibility and ease of maintenance, enabling AUVs to be deployed for extended periods without human intervention [6].

WPT technology necessitates integration with charging platforms to accomplish the energy replenishment tasks for AUVs. The underwater inclusive charging platform has a cage shell. It requires low docking accuracy, and can protect the AUV during the charging process [7], making it widely utilized [8]. To ensure the smooth entry and exit of the AUV, the diameter of the cage of the charging platform is designed to be larger than the AUV itself. Although presetting a particular gap can prevent the AUV from getting stuck during entry and exit, it will also reduce the performance of wireless power transmission.

Researchers have optimized the structure of the magnetic coupler to effectively reduce the impact of external environmental factors on transmission performance. Initially, the magnetic couplers used in AUV wireless power transmission featured transmitters and receivers composed of planar coils [9]. However, their lack of conformity with the AUV's surface structure led to increased transmission distances and excessive space occupation. To address this issue, researchers proposed a magnetic coupler composed of multiple segments of rectangular coils joined together [10]. Although the receiver can conform to the AUV's surface, this design results in significant magnetic leakage from the transmitter, leading to poor coupling performance and unsuitable for high-power transmission. Researchers

Received 6 May 2024; revised 6 August 2024; accepted 29 September 2024. Date of publication 3 October 2024; date of current version 12 December 2024. This work was supported by the Research Grants Council, Hong Kong SAR, China, under Grant CRF-YCRG C1002-23Y. Recommended for publication by Associate Editor X. Ruan. *(Corresponding author: Jiayu Zhou.)*

Ben Zhang and Yong Lu are with the College of Power and Energy Engineering, Harbin Engineering University, Harbin 150001, China (e-mail: zhangben@hrbeu.edu.cn; luyongheu@hrbeu.edu.cn).

C. Q. Jiang and Chen Chen are with the Department of Electrical Engineering, City University of Hong Kong, Hong Kong SAR, China (e-mail: chjiang@cityu.edu.hk; cchen475-c@my.cityu.edu.hk).

Fengshuo Yang is with the School of Electrical Engineering and Automation, Harbin Institute of Technology, Harbin 150001, China (e-mail: 21b906045@stu.hit.edu.cn).

Jiayu Zhou is with the Department of Electrical and Electronic Engineering, The University of Hong Kong, Hong Kong SAR, China (e-mail: jiayzhou@hku.hk).

Color versions of one or more figures in this article are available at https://doi.org/10.1109/TPEL.2024.3473946.

Digital Object Identifier 10.1109/TPEL.2024.3473946

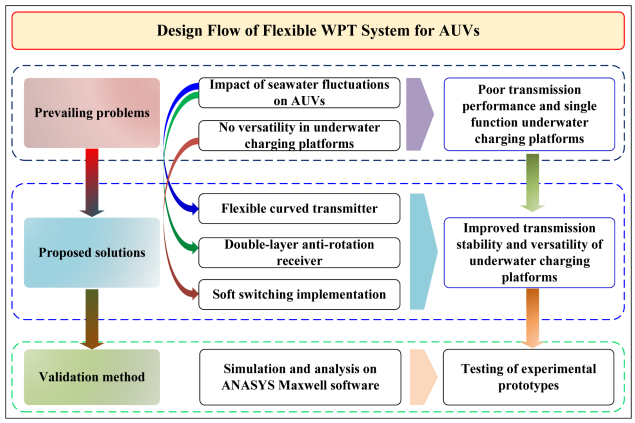

Fig. 1. Design flow and main work of flexible WPT system for AUVs.

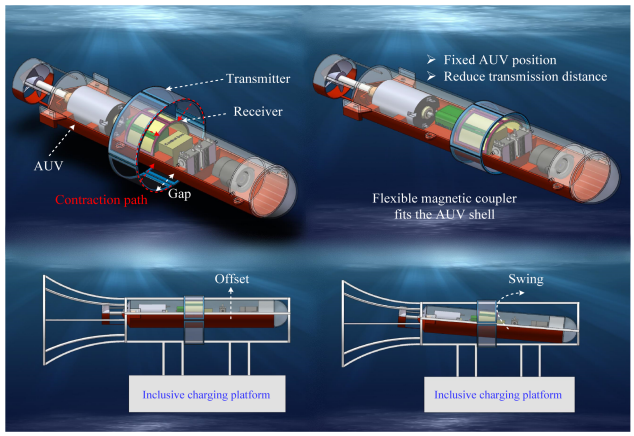

Fig. 2. Application background and structural configuration of underwater inclusive charging platform.

subsequently proposed a plan that features a transmitter with curved coils and a receiver composed of spatial rectangular coils [11]. While this structure demonstrates effective coupling capabilities, the receiver occupies significant space inside the AUV. Designing the transmitter and receiver to conform to the AUV's surface structure may be more effective. Transmitters and receivers of curved coils exhibit good transmission performance and save space [12]. However, their lack of robust antirotation capabilities significantly dampens transmission performance when the AUV undergoes extensive rotation. Although transmitters and receivers comprised of ring coils offer enhanced antirotation capabilities, they are limited by their fixed structural sizes, which reduces their versatility [13].

Based on the above background, the following requirements are proposed for the WPT system applied to AUVs. First, the magnetic coupler structure is flexibly integrated with the platform cage to provide sufficient space for the AUV to enter and exit and to minimize the changes in its position due to seawater fluctuations during the charging process. Second, due to the narrow space inside the charging platform cage, the AUV makes it challenging to adjust the posture, and the transmitter and receiver are frequently not at the optimal centering angle. Therefore, the magnetic coupler should have a strong antirotation capability to address the weakening of the coupling capability when the coils are not aligned, and the magnetic field distribution should be concentrated inside the coupler to avoid electromagnetic interference with the internal devices of the AUV. Finally, a corresponding control strategy should be implemented to ensure the system can guarantee soft switching under any flexible magnetic coupler (FMC) state and output power conditions.

The research line of this article is shown in Fig. 1, and the main contributions are summarized as follows.

1) An FMC is proposed that integrates with underwater inclusive charging platforms, tracking the platform cage's contraction and expansion. It facilitates the AUV's entry and exit from the platform and reduces the transmission distance, thereby completing efficient energy transfer. More importantly, the variable transmitter structure provides the possibility of energy supply for multiple models of AUVs, increasing the versatility of the underwater charging platform.
2) The FMC is optimized for both coil structure and magnetic core layout to obtain excellent antirotation capability. In addition, the FMC's magnetic field is uniformly distributed and concentrated between the magnetic cores of the transmitter and receiver, with little effect on the AUV's internal equipment.
3) The soft switching of WPT systems can be consistently achieved through pulse density modulation (PDM) technology across the entire range of output power. Moreover, for WPT systems that utilize FMC, the mutual inductance and transmitter self-inductance undergo variations. A detuning design is implemented to ensure soft switching in any FMC state.
4) A system prototype is constructed, and the fabrication process is detailed. Emphasis is placed on verifying the FMC's performance and the control's effectiveness.

The rest of this article is organized as follows. Section II introduces the structural principles and demand analysis of FMC. Section III optimizes the antirotation capability of the FMC, and finite element analysis is performed. Section IV elaborates on the control method for coupling parameter changes and different power output conditions. Section V discusses the development and experimental validation of the WPT prototype. Section VI compares the method proposed in this article with similar work. Finally, Section VII concludes this article.

II. Proposal of FMC

A. Structure and Principles

Tides and the Earth's rotation cause fluctuations in seawater. As can be seen from Fig. 2, due to the gap between the AUV and the underwater inclusive charging platform, the position of the AUV will change when it is impacted by seawater. More importantly, it will cause changes in the coupling parameters of the WPT system and affect transmission stability.

To address the issues above, this article proposes an FMC consisting of a single-layer transmitter coil capable of structural

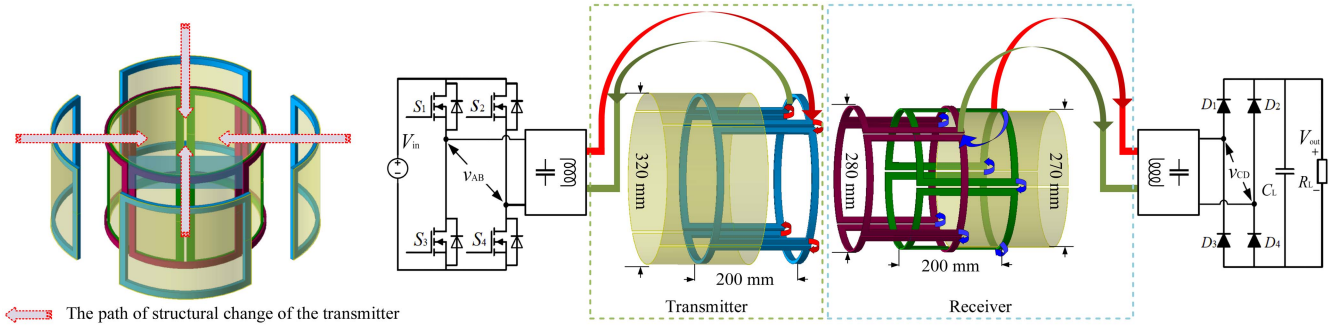

Fig. 3. FMC component distribution and coil connection methods.

changes and an interleaved dual-layer receiver coil, as illustrated in Fig. 3. The transmitter coil is formed by serially connecting multiple curved rectangular coils in the same direction. While adhering to the same principle, the receiver coils are interconnected in series between the two layers, ensuring that all coils have consistent polarity. This FMC structure enhances the transmission efficiency and versatility of the underwater charging platform and improves its antirotation capability.

The principle is that the size can be expanded to its maximum extent to facilitate the entry of an AUV into the underwater inclusive charging platform. Then, the transmitter follows the platform cage as it contracts to a position that fits the surface of the AUV. At the end of charging, the transmitter expands again, leaving plenty of space for the AUV to exit the platform. This flexible transmitter structure reduces the distance over which wireless power can be transmitted and allows efficient energy resupply for a wide range of AUV models [14].

B. Demand Analysis

The analysis of the coupling status of AUV during energy supply on the underwater inclusive charging platform was conducted using ANSYS Maxwell. The transmitter diameter is designed to be 360 mm, the outer receiver diameter is 280 mm, and the inner receiver diameter is 270 mm. The coupling situation changes when the AUV is disturbed by ocean currents, as demonstrated in Fig. 4. The coupling capacity will increase or decrease as the average distance between the transmitter and receiver changes due to offset or swing. When the AUV moves closer to the receiver from a centered position, such as an offset from 0 to 20 mm, the mutual inductance changes by 27%. Interestingly, as the AUV attitude swings, the mutual inductance becomes greater as the magnetic flux through the receiver increases. At its maximum value, the mutual inductance changes by 45%. Thus, developing FMC is essential to enhancing the stability of the charging process.

A finite element analysis was performed to investigate the FMC's magnetic field distribution [15], as shown in Fig. 5. The magnetic field distribution is uneven before the FMC launcher contractions, and the magnetic flux leakage is severe. When the FMC contractions, the transmitter and the receiver are tightly coupled, the magnetic field distribution is uniform, and there is no electromagnetic wave leakage. Among them, the magnetic induction intensity between the transmitter and the receiver is

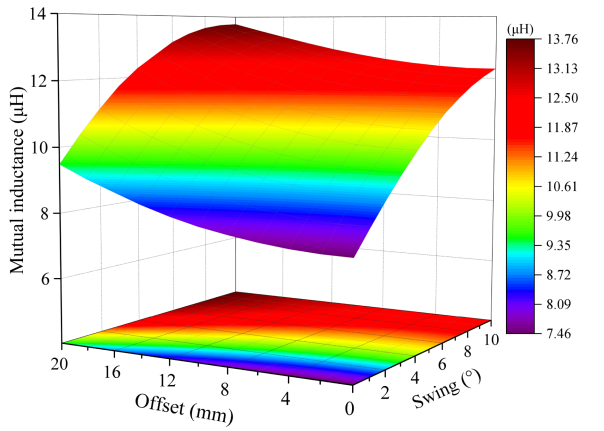

Fig. 4. Variation of coupling parameters at distinct positions of the AUV.

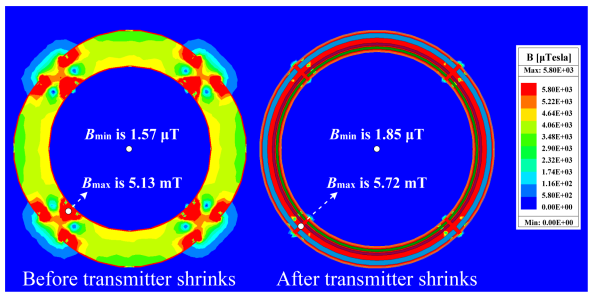

Fig. 5. Magnetic field distribution in different states of FMC.

improved, while the magnetic induction intensity inside the AUV is almost unchanged.

The necessity of double-layer receiving coils is analyzed, as depicted in Fig. 6. When facing the AUV rotation, mutual inductance decreases rapidly if there is no angle difference between the double-layer receiver coils. On the contrary, if there exists an angular difference between the two layers of coils, it can mitigate the mutual inductance drop caused by the rotation of the AUV. Setting up a double-layer receiver coil with an angular difference is significant for resisting the rotation of the AUV.

III. Optimization and Analysis of FMC

The above content introduces the demands and structural principles of FMCs' function. To improve the antirotation ability

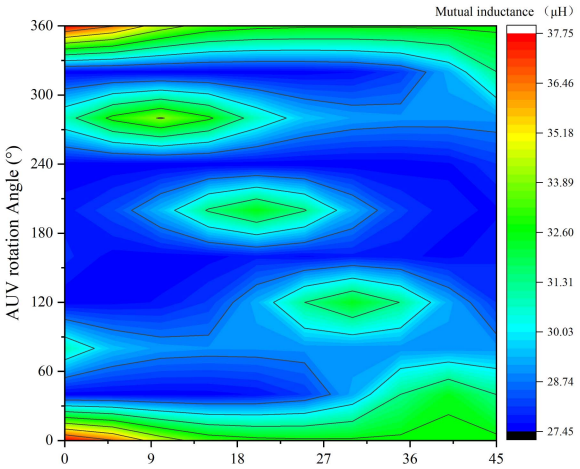

Fig. 6. Analysis of the necessity of a double-layer receiver coil.

of the FMC, the structure will be optimized and analyzed in this session.

A. Antirotation Structure Optimization

Further structure optimization is necessary for an FMC with better antirotation properties. Based on the previous design experience and combined with the former simulation, to maintain the transmitter and receiver inductances similar, the transmitter coil is set up to consist of seven turns, and the receiver includes two layers, and each layer has four turns. To minimize the area occupied by the coil, the transmitter coil is designed with four turns on the upper layer and three turns on the lower layer, all tightly wound.

Fig. 7 analyzes the variations in mutual inductance when the AUV is rotated from 0° to 360°. Fig. 7(a), (b), and (c) shows the variation of mutual inductance when the transmitter coils and each layer of receiver coils consist of four arcs and the two layers of receiver coils are rotated by 0°, 22.5°, and 45°, respectively, between each other. The mutual inductance fluctuations generated by the AUV rotation are larger when there is no angular rotation between the two layers of receiver coils. When the rotation angle between the two layers of receiver coils is 22.5° and 45°, the magnitude of fluctuations in mutual inductance decreases. Notably, the number of fluctuations of the mutual inductance also becomes less when the rotation angle is 45°. As displayed in Fig. 7(d) and (f), when transmitter coils and each layer of receiver coils consist of six arcs or eight arcs, if there is no angle rotation between the two layers of receiver coils, the fluctuations in mutual inductance will be greater than the case when divided into four arcs. Although there exists an angle rotation between the two layers of receiver coils, when the transmitter coils and each layer of receiver coils consist of more arcs, it leads to an increase in the number of fluctuations of mutual inductance, as shown in Fig. 7(d) and (g). Therefore, the transmitter coils and each layer of receiver coils consist of four arcs, with 45° rotation between the two layers of receiver coils as the optimal FMC structure.

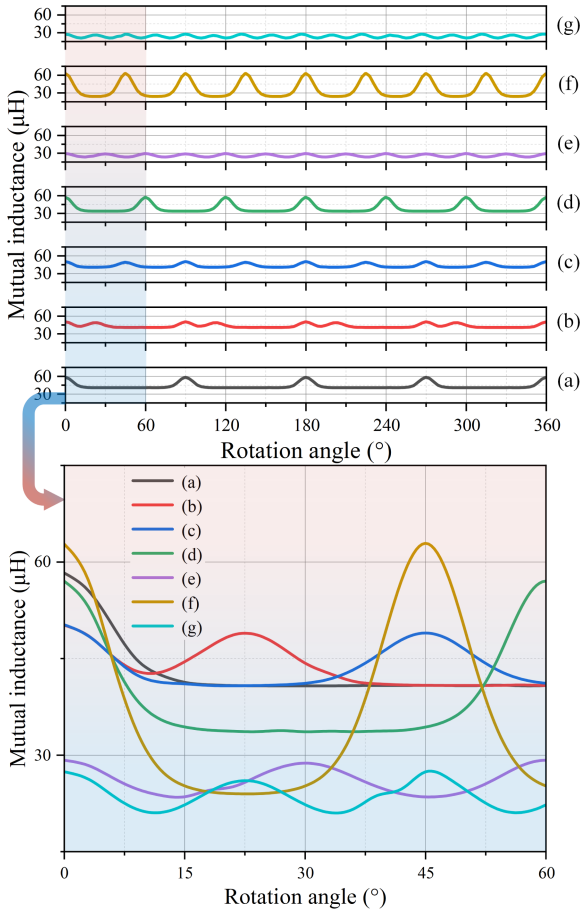

Fig. 7. Variation of mutual inductance during AUV rotation for different magnetic coupler structures. Define P as the number of sets composed of the transmitter and receiver, and R as the angular difference between the double-layer coils of the receiver. (a) P is 4 and R is 0°. (b) P is 4 and R is 22.5°. (c) P is 4 and R is 45°. (d) P is 6 and R is 0°. (e) P is 4 and R is 30°. (f) P is 8 and R is 0°. (g) P is 4 and R is 22.5°.

Once the structure of the FMC is determined, it is necessary to optimize the arrangement of the magnetic core. To enhance the power density of the magnetic coupler, we use a thinner and lighter 0.2 mm nanocrystalline ribbon as the core material. We simulate and compare the coupling parameters of different magnetic core arrangements, as given in Table I. Since the magnetic core can provide a gathering effect, adding them on the inside of the receiver and the outside of the transmitter is most effective. While keeping the total number of nanocrystalline cores (also the total weight) constant, the areas and thicknesses of different arrangements were compared. By comparison, it is found that the coupling performance is optimal when the magnetic core covers the entire surface.

B. Finite-Element Analysis

Through optimization analysis, the antirotation ability is the best when the double-layer receiver coil is in an orthogonal position. This structure helps to eliminate the mutual coupling between windings. In this structure, the coupling ability is strongest when the transmitter's outer and receiver's inner sides completely cover the magnetic core.

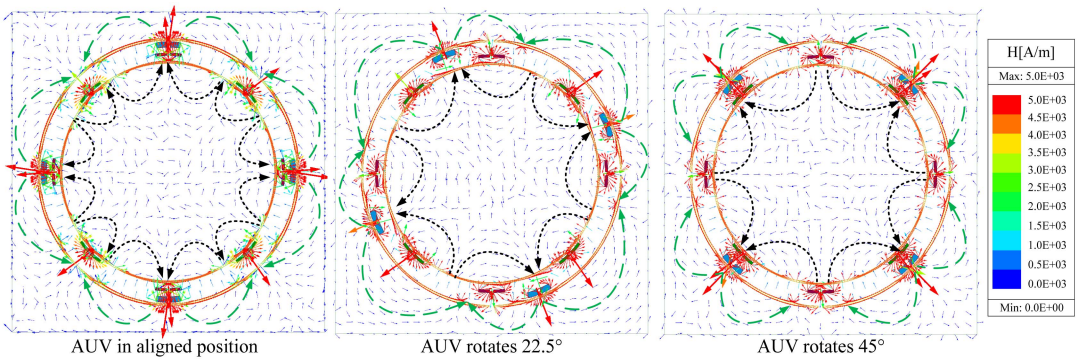

Fig. 8. Magnetic field intensity vector distribution of FMC when AUV rotates at 0°, 11.25°, and 22.5°.

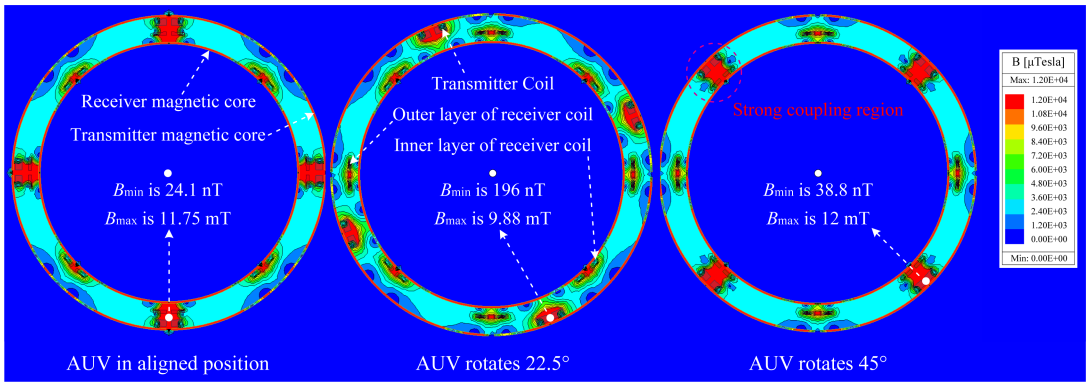

Fig. 9. Magnetic induction intensity distribution of FMC when AUV rotates at 0°, 11.25°, and 22.5°.

TABLE I
COMPARISON OF DIFFERENT MAGNETIC CORE ARRANGEMENT METHODS

Parameters	(a)	(b)	(c)
Model example	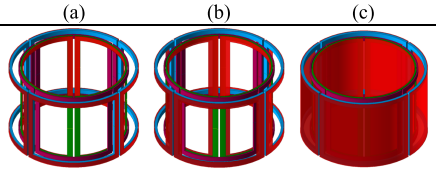		
Transmitter coil self-inductance (μH)	77.92	84.06	94.52
Receiver coil self-inductance (μH)	72.59	77.51	89.03
Mutual inductance (μH)	21.52	24.27	32.82
Coupling coefficient	0.29	0.30	0.36

(a) Same width as single-side coil, magnetic core thickness 1.2 mm. (b) Double width of single-side coil, core thickness 0.6 mm. (c) Magnetic cores cover the entire surface with a thickness of 0.2 mm.

An excitation current with an amplitude of 20 A is applied to the winding of the FMC. The distribution of the magnetic field during the AUV's rotation is analyzed using finite element analysis [16]. Fig. 8 shows the distribution of the magnetic field intensity vectors. The magnetic lines of force in the two adjacent transmitter coils are in opposite directions. The centers of the four transmitter coils act as magnetic poles, interconnected through a magnetic core. The main magnetic flux passes through the center of the transmitter coils, enters the receiver, and then returns to the two ends of the transmitter coils. As the AUV rotates, the position of the main magnetic flux shifts correspondingly.

Due to the numerous precision instruments used for navigation inside the AUV, special attention is required to manage the magnetic leakage of the magnetic coupler. The distribution of magnetic induction intensity of the FMC is illustrated in Fig. 9. When the AUV is aligned, the transmitter and outer layer of receiver coils create a strong coupling region. At a 22.5° rotation, all coils show strong coupling at both ends, but with reduced intensity. At a 45° rotation, the transmitter coils form a strong coupling region with the inner layer of receiver coil, and the overall distribution resembles the aligned position. When the AUV is centered, the maximum magnetic induction intensity between the transmitter and receiver is 11.75 mT, while the minimum at the central position is 24.1 nT. As the AUV rotates, these extreme magnetic induction values remain largely unchanged, effectively demonstrating this structure's exceptional magnetic shielding capability.

Fig. 10 illustrates the reluctance model of the proposed FMC. Due to the symmetry of FMC, only a quarter part is taken for analysis. Among them, F_p is the magnetomotive force generated by the transmitter, and F_s is the induced magnetomotive force of the receiver. Φ_{p} represents the self-coupling magnetic flux of the transmitter, Φ_s represents the self-coupling magnetic flux of the receiver, and Φ_m represents the mutual coupling magnetic

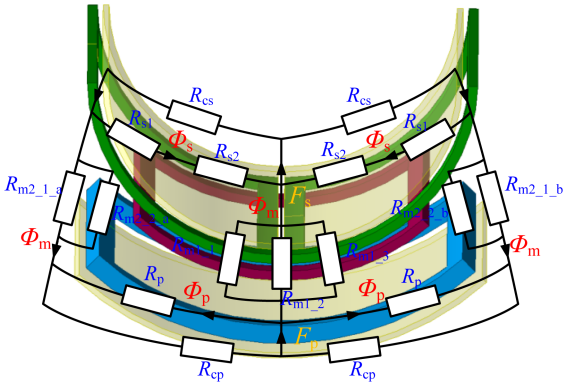

Fig. 10. Reluctance model of the proposed flexible magnetic coupler.

flux of the magnetic coupler. R_{cp} is the core reluctance of the transmitter, and R_{cs} is the core reluctance of the receiver. R_p is the emitter self-coupling region reluctance. R_{s1} and R_{s2} represent the self-coupling area reluctance of the receiver double-layer coil. R_m represents the mutual coupling area reluctance.

Define the number of turns of the transmitter coil as N_p, the number of turns of the outer coil of the receiver as N_{s1}, and the number of turns of the inner coil as N_{s2}. The relationship between leakage inductance and reluctance of FMC is as follows:

$$\begin{cases} L_{p\_\text{lea}} = \dfrac{N_p^2}{R_p} \\ L_{s\_\text{lea}} = \dfrac{(N_{s1}+N_{s1})^2}{R_{s1}+R_{s2}} \end{cases} \tag{1}$$

where L_{p_lea} is the leakage inductance of the transmitter, and L_{s_lea} is the leakage inductance of the receiver.

Then, the calculation equations for the self-inductance, mutual inductance, and coupling coefficient of the FMC are derived as follows:

$$\begin{cases} L_p = L_{p\_\text{lea}} + M = \dfrac{N_p^2}{R_p} + \dfrac{N_p(N_{s1}+N_{s2})}{R_m} \\ L_s = L_{s\_\text{lea}} + M = \dfrac{(N_{s1}+N_{s1})^2}{R_{s1}+R_{s2}} + \dfrac{N_p(N_{s1}+N_{s2})}{R_m} \\ M = \dfrac{N_p(N_{s1}+N_{s2})}{R_m} \\ R_m = R_{m1\_1} + R_{m1\_2} + R_{m1\_3} + R_{m2\_1\_a} \\ \qquad +R_{m2\_2\_a} + R_{m2\_1\_b} + R_{m2\_2\_b} \end{cases} \tag{2}$$

$$k = \sqrt{\frac{M}{L_p}\cdot\frac{M}{L_s}} = \sqrt{\frac{N_p\left(N_{s1}+N_{s2}\right)}{\left(\frac{N_pR_m}{R_p}+N_s\right)\left(\frac{(N_{s1}+N_{s2})R_m}{R_{s1}+R_{s2}}+N_p\right)}} \tag{3}$$

where k is the coupling coefficient.

It can be seen from (2) and (3) that after the structural parameters of the FMC are determined, the degree of coupling mainly depends on the inductance of the self-coupling region and the mutual coupling region.

When the FMC receiver rotates, due to the convergence of the magnetic field by the magnetic cores on both sides, the length of the magnetic circuits included in R_{m1_1}, R_{m1_2}, and R_{m1_3} changes slightly. The reluctance $R_{m\_2\_1\_a}$ and $R_{m\_2\_2\_a}$ on the left side of the receiver are complementary to the reluctance

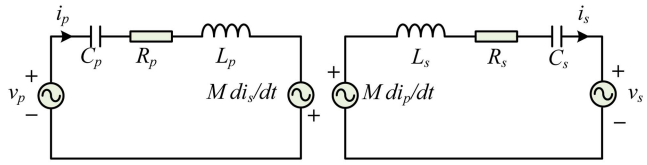

Fig. 11. Equivalent circuit of series-series compensated WPT system using first harmonic approximation.

$R_{m\_2\_1\_b}$ and $R_{m\_2\_2\_b}$ on the right side. Therefore, the sum of mutual inductance and reluctance remains basically constant, laying the foundation for the stability of FMC mutual inductance. In summary, the FMC can utilize its structural advantages to enhance its antirotation capability.

IV. Ensuring Soft Switching for Systems With FMC

In WPT systems equipped with a FMC, ensuring soft switching under various operating conditions, including variable coupling configurations and output power, is paramount [17]. While phase shift modulation (PSM) is a common modulation strategy that offers simplicity, it typically sacrifices soft switching under light load conditions [18]. Conversely, PDM regulates system power through pulse skipping, effectively achieving soft switching across the entire power range [19]. Therefore, this article employs PDM to guarantee soft switching while managing the system's output power. Notably, a significant challenge in WPT systems with an FMC lies in achieving soft switching under varying coupler states, where both mutual inductance M and transmitter self-inductance L_p can vary concurrently. This aspect has not been comprehensively addressed in previous WPT systems utilizing PDM.

A. Power Regulation by PDM

Based on the first harmonic approximation [20], the equivalent circuit for the series-series compensated WPT system is depicted in Fig. 11. It includes v_p (v_s), i_p (i_s), L_p (L_s), C_p (C_s), R_p (R_s), and M, representing transmitting (receiving) voltage, current, inductance, capacitance, series-equivalent resistances, and mutual inductance. When considering the steady-state charging of a battery via a high-frequency resonant converter, the battery can be approximated as a voltage load. In this scenario, the receiving voltage (v_s) of the system is in phase with the receiving current (i_s) due to the diode rectifier, and its amplitude is determined by the output dc voltage:

$$\begin{cases} |v_s| = \dfrac{2\sqrt{2}}{\pi}\cdot V_{\text{dc,out}} \\ \angle v_s = \angle i_s \end{cases} \tag{4}$$

where $V_{\text{dc\_out}}$ is the battery voltage on the output side.

The PDM scheme features a distinctive pulse pattern, as illustrated in Fig. 12. While pulse generation in PDM can be achieved through delta sigma modulation to facilitate continuous density adjustments [21], this aspect is not explored in this article due to space constraints. Moreover, the ratio of remaining pulses to total switching cycles defines the pulse density, denoted by D. By adjusting D, one can regulate the average output power in WPT systems employing PDM, without impacting the input

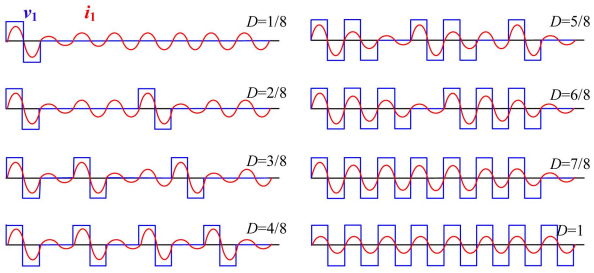

Fig. 12. Transmitting voltage and transmitting current of the WPT system with different densities when using PDM.

impedance angle. This approach mitigates the adverse effects of increased switching losses stemming from the absence of zero voltage switching (ZVS) during voltage control via PSM. Therefore, by manipulating D, the transferred power in a PDM-based system can be formulated as follows:

$$P_{\text{in}} = \frac{2\sqrt{2}}{\pi} \cdot D \cdot V_{\text{dc\_in}} \cdot i_p \cdot \cos\left(\theta_{\text{input}}\right) \tag{5}$$

where θ_{input} denotes the phase angle between the transmitting voltage and the transmitting current.

B. Ensuring Soft Switching

To achieve soft switching, it is desirable for the input current to exhibit inductive behavior when the switch activates, which corresponds to θ_{input} being larger than zero. Systems equipped with fixed couplers can operate at a slightly super-resonant frequency [22] or by detuning the resonators [23] to facilitate ZVS. However, the aforementioned approaches are typically tailored for fixed couplers and have not been delved into in the context of the flexible couplers presented in this article. To demonstrate their viability, the system's unbalanced factor x_u and detuning factor x_c are defined as follows:

$$\begin{cases} x_u = \sqrt{\frac{L_p}{L_s}} \frac{V_s}{V_p} \\ x_c = \frac{C_p \cdot L_p}{C_s \cdot L_s} \end{cases}. \tag{6}$$

When considering a lossless system, the input impedance angle of the system can be determined by combining the equivalent circuit depicted in Fig. 11 with (4), (5), (6)

$$\theta_{\text{input}} = \arctan\left(\frac{\left(1 - \frac{\omega_p^2}{\omega^2}\right) - \frac{1}{x_u^2}\left(1 - \frac{x_c^2 \cdot \omega_p^2}{\omega^2}\right)}{\sqrt{\frac{k^2}{x_u^2} - \left(1 - \frac{\omega_p^2}{\omega^2}\right)^2}} \right) \tag{7}$$

where ω_p is the resonant frequency of the transmitting side of the system and ω is the operating frequency in the system.

By taking the partial derivative of the operating frequency in the preceding formula, we can derive the subsequent equation as follows:

$$\frac{\partial \tan(\theta_{\text{input}})}{\partial \omega} = \frac{2\omega_p^2 k^2 \omega^3 (x_u^2 - 1) + 2\omega_p^2 \omega x_u^2 (\omega^2 - \omega_p^2)(x_c - 1)}{x_u (k^2 \omega^4 - x_u^2 (\omega^2 - \omega_p^2)^2)^{3/2}}. \tag{8}$$

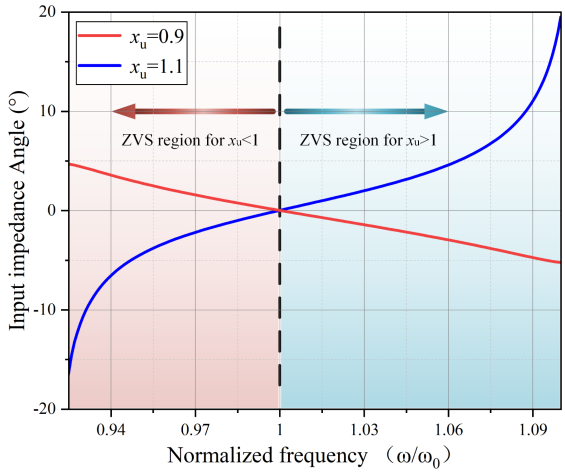

Fig. 13. Input impedance angle of the WPT system under different x_u.

When the system is not detuned (i.e., $x_c = 1$), the input impedance angle exhibits a monotonic relationship with frequency, which is influenced by the value of x_u. Fig. 13 illustrates the input impedance angles of the system across various values of x_u. Observations reveal that for x_u greater than 1, the system experiences a monotonic increase, while for x_u less than 1, there is a monotonic decrease. This behavior aligns with the conclusions drawn from (8). However, for the systems with FMC, x_u is highly variable and can fluctuate above and below 1 due to variations in L_p. Therefore, the system's ZVS region shifts within both the super-resonant and subresonant frequency domains, as depicted in Fig. 13. Given these considerations, it is unsuitable for the WPT system with FMC addressed in this article to operate at nonresonant frequencies to achieve soft switching. Therefore, the detuning design approach should be considered. In this scenario, the input impedance angle of the system when it operates at the receiving side's resonant frequency is given as follows:

$$\theta_{\text{input}} = \arctan\left(\frac{\left(1 - \frac{1}{x_c^2}\right)}{\sqrt{\frac{k^2}{x_u^2} - \left(1 - \frac{1}{x_c^2}\right)^2}} \right). \tag{9}$$

It is noteworthy that the resonant frequency of the transmitting side is not employed due to the flexible coupler's propensity to induce variations in L_p under differing operational conditions, subsequently altering the resonant frequency. Conversely, the receiving side maintains a constant resonant frequency. As evident from (9), when x_c surpasses 1, the input impedance angle consistently remains above 0, remaining unaffected by both x_u and k, and thus, remains impervious to coupler rotations. Fig. 14 illustrates the system's input impedance angle when x_c is 1.03, revealing that it consistently exceeds 0 in a wide range of x_u and k. Moreover, when the transmitter coil has expansions, resulting in a larger L_p, x_c continues to increase. Therefore, the system retains its capability to execute soft switching, highlighting the advantage of the detuning design approach in WPT systems

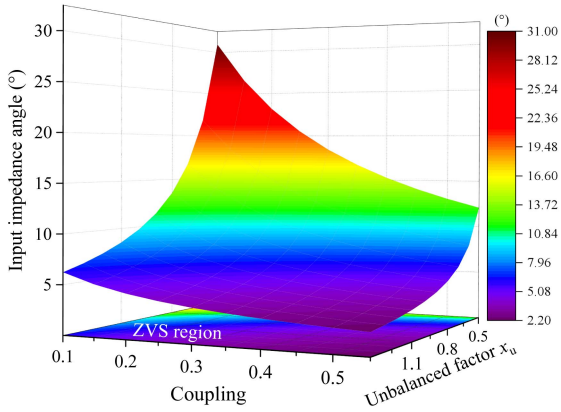

Fig. 14. Input impedance angle of detuned WPT system ($x_c = 1.03$) at resonant frequency with different x_u and k values.

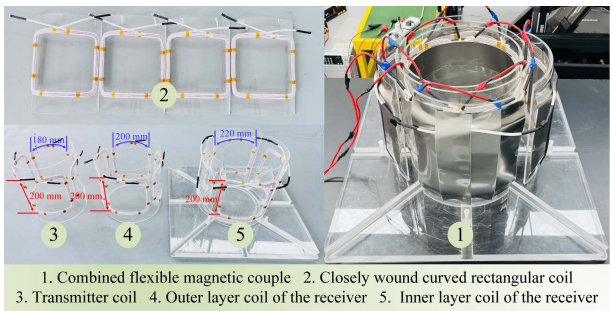

Fig. 15. Coil structural composition and overall layout of FMC.

featuring FMC. This assertion will be substantiated in the subsequent experimental section.

V. Experimental Validation

A 1 kW WPT prototype was constructed to validate the FMC and the presented control method. This section provides a detailed description of the prototype's fabrication process and conducts comprehensive functional validation of the prototype. In previous work [24], we have explored that at an operating frequency of 100 kHz, the transmission performance of WPT in a seawater environment is almost equivalent to that in an air environment. Therefore, seawater environmental experiments will no longer be carried out in this article to speed up the research progress.

Based on the optimized simulation results, the FMC's structure was constructed as depicted in Fig. 15. This FMC employs 0.1 mm × 800 strands of Litz wire and utilizes a 0.2 mm thick nanocrystalline strip as the magnetic core. The diameters of the transmitter coil, the outer layer of the receiver coil, and the inner layer of the receiver coil are 320, 280, and 270 mm, respectively. The transmitter coil consists of seven turns, while both layers of receiver coils comprise four turns each, all with a height of 200 mm. Each layer of the coupler comprises four curved coils, each with an arc of 90°, and the coils are connected in series. An acrylic base was designed to simulate the flexibility of the magnetic coupler, allowing for the expansion and contraction of the transmitter coil and angular rotation of the receiver coils on the base.

TABLE II
Parameters of Prototype Coupler (in Fitting State)

Parameters	Value
Transmitter coil inductance L_p	94 μH
Receiver coil inductance L_s	82.9 μH
Internal resistance of transmitter coil R_p	305 mΩ
Internal resistance of receiver coil R_s	282 mΩ
Mutual inductance M	31.24 μH
Initial detuning factor x_c	1.04

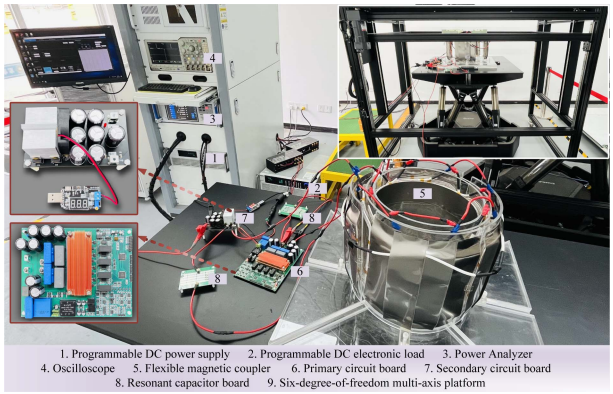

Fig. 16. Composition of the WPT system prototype and the distribution of the experimental environment.

The parameters of the FMC are given in Table II. To facilitate the winding process, an acrylic shell was added between the two layers of receiver coils, resulting in a decrease in the self-inductance of the receiver coils and the mutual inductance between the couplers compared to the simulated values.

The optimal resonant frequency for the prototype system was established at 100 kHz. The prototype's distribution and the experimental environment are depicted in Fig. 16. The prototype utilizes a Chroma 62 000 H programmable dc power supply to provide energy input to the primary circuit, while the output energy from the secondary circuit is directed to a Chroma 63 200 A dc electronic load. A LECROY WaveSurfer 4000 HD high-precision oscilloscope captures waveforms at critical locations within the system. To analyze the energy transfer within the system, a HIOKI PW6001 power analyzer is utilized. The primary circuit includes a full-bridge inverter module, a signal processing module, a low-power supply module, an output current acquisition module, and an output voltage acquisition module. This design adheres to the principle of miniaturization, resulting in space-saving. To ensure a compact design, an external fan is added to the secondary circuit to improve the heat dissipation capacity.

A. FMC Dimension Variation

Using a six-degree-of-freedom multiaxis platform, we tested the transmission performance variation of the WPT system before contracting the transmitter structure (with a diameter of 360 mm). The receiver's centered position is defined as (0, 0),

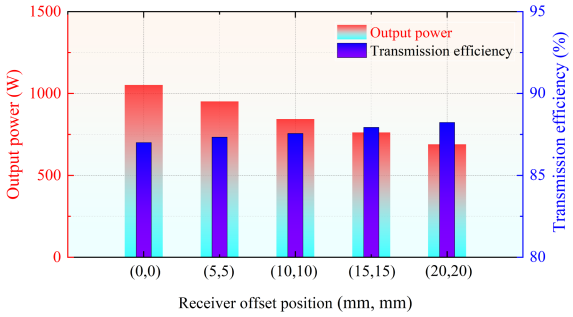

Fig. 17. Impact of receiver offset on system transmission performance before transmitter contraction.

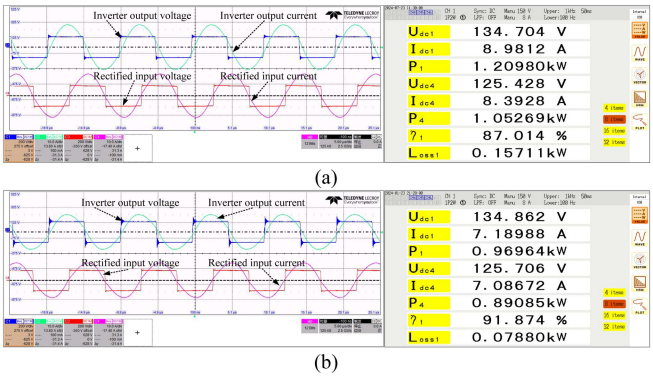

Fig. 18. System waveform and power analysis. (a) Transmitter far from AUV. (b) Transmitter fits AUV.

and its position after shifting x mm along the X-axis and y mm along the Y-axis is defined as (x, y). The transmission performance at various receiver positions was observed by keeping the power supply voltage at 135 V and the load resistance at 5 Ω constant, as illustrated in Fig. 17. As the receiver contracts, the mutual inductance slightly increases. Consequently, the system's transmission efficiency increases while the output power decreases, which is consistent with the characteristics of the S-S resonant compensation network.

When the FMC begins operation, its transmitter contracts to a diameter of 300 mm. A comparison of the transmission performance of the WPT system in two states is shown in Fig. 18. The inverter outputs a square wave with a 50% duty cycle, achieving good soft switching. In the 125 V constant voltage output mode, the coupling coefficient and mutual inductance increase as the transmitter contracts, leading to an overall dc–dc transmission efficiency improvement of 4.86%.

B. FMC Antirotation Characteristics

The FMC we proposed demonstrates excellent antirotation capabilities. From Fig. 7(a), it can be observed that one complete cycle of AUV rotation occurs at 45°. Considering half a cycle, the system performance at three positions – 0°, 11.25°, and 22.5° - is compared, as depicted in Fig. 19. When the AUV is aligned at the center (0°), the system achieves its highest transmission efficiency, reaching 91.87%. As the rotation angle increases, the coupling coefficient and mutual inductance decrease slightly,

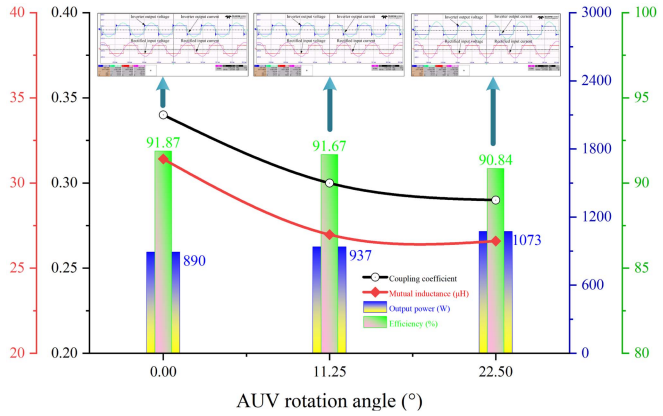

Fig. 19. Comparison of WPT system performance when the AUV rotates 0°, 11.25°, and 22.5°.

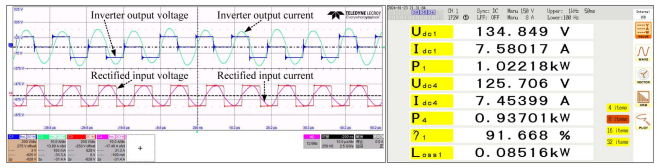

Fig. 20. WPT system waveform and power analysis under a light load condition ($D = 0.6$).

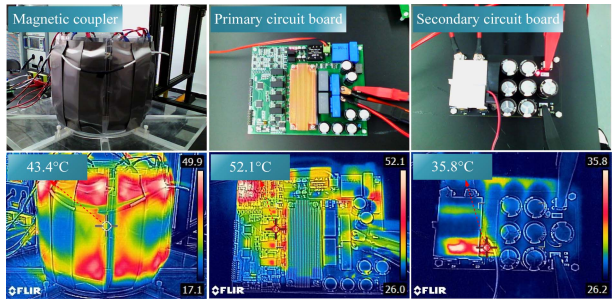

Fig. 21. Temperature distribution of WPT system prototype.

reducing system efficiency. Due to its outstanding antirotation capabilities, the maximum decrease in system efficiency is only 1.03%. More importantly, the system can achieve soft switching when the AUV rotates to any angle.

C. Light Load Performance and System Temperature

Fig. 20 shows the experimental result of the system at $D = 0.6$, enabling soft switching. The system performs similarly in other light load conditions, guaranteeing soft switching and high efficiency. During the system's operation, each component's temperature distribution was observed using a thermal imaging camera, as shown in Fig. 21. The temperature distribution of the magnetic core in the magnetic coupler is uniform, with the highest temperature observed at the edges, reaching 49.9 °C. The primary and secondary circuit boards of the system are equipped with efficient heat dissipation modules, ensuring that the temperature is controlled at a low level.

TABLE III
COMPARISON BETWEEN PROPOSED METHOD AND SIMILAR WORKS

Display view	Reference	Power level	Efficiency	Anti-rotation ability
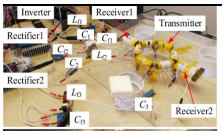	Zhang et al. [10]	500 W	90%	★★
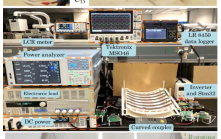	Chen et al. [12]	1000 W	92.85%	N/A
	Wu et al. [15]	960 W	90.9%	★
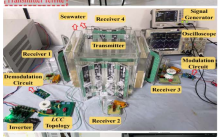	Zeng et al. [25]	200 W	92.25%	★
	This article	890 W	91.87%	★★★

VI. COMPARISON WITH SIMILAR WORK

The comparison of the data from this article with similar research is given in Table III. The output power and transmission efficiency of the WPT system designed in this article have reached current standards. Notably, the FMC proposed in this article is a novel method for integration with underwater charging platforms, enhancing the stability of WPT system transmission and the versatility of underwater charging platforms. Additionally, based on the FMC structure, antirotation optimization has been carried out, effectively addressing the issue of low efficiency when there is an angle difference between the coils.

VII. CONCLUSION

This article proposes a novel antirotational FMC for WPT systems to AUVs. The structure of the transmitter allows for adaptation to the adjustable cage of the charging platform. By optimizing, the FMC consisting of a single-layer transmitter coil and a double-layer receiver coil with a 45° rotation between receiver layers, it shows excellent antirotation capability over a 360° range. Additionally, the FMC's magnetic field is uniformly distributed and concentrated between the coupler's magnetic cores, minimizing interference with the AUV's internal equipment. To address the resonance state changes caused by coupling parameter variations during the operation of the FMC, PDM, and detuning design of resonators are introduced to realize soft switching in the presented WPT system. Experimental results show that, while maintaining an output power of 890 W, the contraction of the FMC's transmitter can increase the system's dc–dc efficiency by 4.86%. Moreover, the system soft switching is realized when the AUV undergoes a rotation of 360°, and the maximum fluctuation in efficiency is only 1.03%.

REFERENCES

[1] C. R. Teeneti, T. T. Truscott, D. N. Beal, and Z. Pantic, "Review of wireless charging systems for autonomous underwater vehicles," *IEEE J. Ocean. Eng.*, vol. 46, no. 1, pp. 68–87, Jan. 2021.

[2] B. Zhang, W. Xu, C. Lu, Y. Lu, and X. Wang, "Review of low-loss wireless power transfer methods for autonomous underwater vehicles," *IET Power Electron*, vol. 15, no. 9, pp. 775–788, Mar. 2022.

[3] Z. Zhang, H. Pang, A. Georgiadis, and C. Cecati, "Wireless power transfer—An overview," *IEEE Trans. Ind. Electron.*, vol. 66, no. 2, pp. 1044–1058, Feb. 2019.

[4] H. Feng, R. Tavakoli, O. C. Onar, and Z. Pantic, "Advances in high-power wireless charging systems: Overview and design considerations," *IEEE Trans. Transp. Electrific.*, vol. 6, no. 3, pp. 886–919, Sep. 2020.

[5] S. Y. Chu, X. Cui, X. Zan, and A.-T. Avestruz, "Transfer-power measurement using a non-contact method for fair and accurate metering of wireless power transfer in electric vehicles," *IEEE Trans. Power Electron.*, vol. 37, no. 2, pp. 1244–1271, Feb. 2022.

[6] D. Wang, J. Zhang, S. Cui, Z. Bie, F. Chen, and C. Zhu, "The state-of-the-arts of underwater wireless power transfer: A comprehensive review and new perspectives," *Renew. Sustain. Energy Rev.*, vol. 189, pp. 113910–113910, Jan. 2024.

[7] C. Cai, J. Li, S. Wu, Z. Qin, W. Chai, and S. Yang, "A bipolar and unipolar magnetic channel multiplexed WPT system with simultaneous full-duplex communication for autonomous underwater vehicles," *IEEE Trans. Power Electron.*, vol. 38, no. 12, pp. 15086–15090, Dec. 2023.

[8] Y. Wang, T. Li, M. Zeng, J. Mai, P. Gu, and D. Xu, "An underwater simultaneous wireless power and data transfer system for AUV with high-rate full-duplex communication," *IEEE Trans. Power Electron.*, vol. 38, no. 1, pp. 619–633, Jan. 2023.

[9] J. Li, C. Zhu, J. Xie, F. Lu, and X. Zhang, "Design and implementation of high-misalignment tolerance WPT system for underwater vehicles based on a variable inductor," *IEEE Trans. Power Electron.*, vol. 38, no. 10, pp. 11726–11737, Oct. 2023.

[10] Y. Zhang, K. Zhang, L. Qiao, Y. Hu, and B. Song, "A multiload wireless power transfer system with concentrated magnetic field for AUV cluster system," *IEEE Trans. Ind. Appl.*, vol. 58, no. 1, pp. 1307–1314, Jan. 2022.

[11] S. Wu, C. Cai, A. Wang, Z. Qin, and S. Yang, "Design and implementation of a uniform power and stable efficiency wireless charging system for autonomous underwater vehicles," *IEEE Trans. Ind. Electron.*, vol. 70, no. 6, pp. 5674–5684, Jun. 2022.

[12] C. Chen, C. Q. Jiang, Y. Wang, Y. Fan, B. Luo, and Y. Cheng, "Compact curved coupler with novel flexible nanocrystalline flake ribbon core for autonomous underwater vehicles," *IEEE Trans. Power Electron.*, vol. 39, no. 1, pp. 53–57, Jan. 2024.

[13] A. Mostafa, Y. Wang, S. Tangirala, H. Zhang, and F. Lu, "A 5 kW hull-compatible inductive charging system with 360°folded spatial unipolar coupler for autonomous underwater vehicles (AUVs)," *IEEE Trans. Ind. Appl.*, vol. 59, no. 6, pp. 7001–7012, Nov. 2023.

[14] B. Zhang, J. Chen, X. Wang, W. Xu, C. Lu, and Y. Lu, "High-power-density wireless power transfer system for autonomous underwater vehicle based on a variable ring-shaped magnetic coupler," *IEEE Trans. Transp. Electrific.*, vol. 10, no. 2, pp. 3061–3074, Jun. 2024.

[15] S. Wu, C. Cai, W. Chai, J. Li, Q. Cui, and S. Yang, "Uniform power IPT system with quadruple-coil transmitter and crossed dipole receiver for autonomous underwater vehicles," *IEEE Trans. Ind. Appl.*, vol. 58, no. 1, pp. 1289–1297, Jan. 2022.

[16] C. Cai, S. Wu, Z. Zhang, L. Jiang, and S. Yang, "Development of a fit-to-surface and lightweight magnetic coupler for autonomous underwater vehicle wireless charging systems," *IEEE Trans. Power Electron.*, vol. 36, no. 9, pp. 9927–9940, Sep. 2021.

[17] C. Cai et al., "Multi-state voltage balancing of UAV's cell string: A reconfigurable WPT based multiport hybrid charging approach," *IEEE Trans. Ind. Electron.*, to be published, doi: 10.1109/TIE.2024.3401190.

[18] X. Wang, J. Xu, M. Leng, H. Ma, and S. He, "A hybrid control strategy of LCC-S compensated WPT system for wide output voltage and ZVS range with minimized reactive current," *IEEE Trans. Ind. Electron.*, vol. 68, no. 9, pp. 7908–7920, Sep. 2021.

[19] X. Wang, C. Q. Jiang, T. Ma, J. Xiang, C. Chen, and K. T. Chau, "Pulse density modulated three-phase single-stage AC–AC system for series resonant load with low grid current harmonics," *IEEE Trans. Ind. Electron.*, vol. 71, no. 5, pp. 4407–4418, May 2024.
[20] C. Cai, J. Wang, M. Saeedifard, P. Zhang, R. Chen, and J. Zhang, "Gyrator-gain variable WPT topology for MC-unconstrained CC output customization using simplified capacitance tuning," *IEEE Trans. Ind. Electron.*, vol. 71, no. 4, pp. 3594–3605, Apr. 2024.
[21] H. Li, J. Fang, S. Chen, K. Wang, and Y. Tang, "Pulse density modulation for maximum efficiency point tracking of wireless power transfer systems," *IEEE Trans. Power Electron.*, vol. 33, no. 6, pp. 5492–5501, Jun. 2018.
[22] Y. Jiang, L. Wang, Y. Wang, J. Liu, M. Wu, and G. Ning, "Analysis, design, and implementation of WPT system for EV's battery charging based on optimal operation frequency range," *IEEE Trans. Power Electron.*, vol. 34, no. 7, pp. 6890–6905, Jul. 2019.
[23] G. Guidi and J. A. Suul, "Minimizing converter requirements of inductive power transfer systems with constant voltage load and variable coupling conditions," *IEEE Trans. Ind. Electron.*, vol. 63, no. 11, pp. 6835–6844, Nov. 2016.
[24] B. Zhang, X. Wang, C. Lu, Y. Lu, and W. Xu, "A wireless power transfer system for an autonomous underwater vehicle based on lightweight universal variable ring-shaped magnetic coupling," *Int. J. Circuit Theory Appl.*, vol. 51, no. 6, pp. 2654–2673, Feb. 2023.
[25] Y. Zeng, C. Lu, R. Liu, X. He, C. Rong, and M. Liu, "Wireless power and data transfer system using multidirectional magnetic coupler for swarm AUVs," *IEEE Trans. Power Electron.*, vol. 38, no. 2, pp. 1440–1444, Feb. 2023.

Ben Zhang (Graduate Student Member, IEEE) is currently working toward the Ph.D. degree in power engineering and engineering thermophysics with the College of Power and Energy Engineering, Harbin Engineering University, Harbin, China.

He has been a Visiting Doctoral Student with the Department of Electrical Engineering, City University of Hong Kong, Hong Kong. Since 2020, he has been engaged in research on wireless power transfer technology for autonomous underwater vehicles. His research focus includes WPT magnetic coupler design, WPT system control methodology studies, and the application of WPT systems in seawater environments.

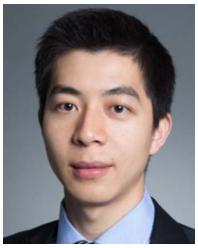

C. Q. Jiang (Senior Member, IEEE) received the B.Eng. and M.Eng. degrees (First Class Hons.) in electrical engineering and automation from Wuhan University, Wuhan, China, in 2012 and 2015, respectively, and the Ph.D. degree in electrical and electronic engineering from The University of Hong Kong, Hong Kong, in 2019.

He is currently an Assistant Professor with the Department of Electrical Engineering, faculty member in the State Key Laboratory of Terahertz and Millimeter Waves, City University of Hong Kong, Hong Kong. From 2019 to 2021, he was a Postdoctoral Research Associate at the University of Cambridge, Cambridge, U.K. Also, he has been affiliated with Clare Hall, University of Cambridge since 2021. In 2019, he was a Visiting Researcher with the Nanyang Technological University, Singapore. His research interests include power electronics, wireless power transfer, electric machines and drives, and electric vehicle technologies.

Dr. Jiang was the recipient of CENG Research Excellence Award, Gold Medal at the Silicon Valley International Invention Festival, Gold Medals with Congratulations of the Jury in International Exhibition of Inventions of Geneva, Winner of CAPE Acorn Blue Sky Research Award at the University of Cambridge, Gold Medal in 3rd Asia Exhibition of Innovations and Inventions, Silver Award and Bronze Award in Shenzhen Qianhai Youth Innovation and Entrepreneurship Competition, and First Prize in the Interdisciplinary Research Competition at the University of Hong Kong. He is currently an Associate Editor for *IET Renewable Power Generation*, a Guest Editor for IEEE OPEN JOURNAL OF VEHICULAR TECHNOLOGY, and IEEE TRANSACTIONS ON POWER ELECTRONICS LETTERS.

Fengshuo Yang received the B.S. degree in instrumentation science and engineering in 2021 from the Harbin Institute of Technology, Harbin, China, where he is currently working toward the Ph.D. degree in electrical engineering with the School of Electrical Engineering and Automation.

His research interests primarily focus on wireless power transfer technology, particularly for applications in AUVs and UAVS.

Chen Chen received the B.Eng. and M.Eng. degrees in mechanical manufacture and automation from the Wuhan University of Technology, Wuhan, China, in 2019 and 2022, respectively. He is currently working toward the Ph.D. degree in electrical engineering with the Department of Electrical Engineering, City University of Hong Kong, Hong Kong.

His research interests include wireless power transfer modeling and control, and power electronics.

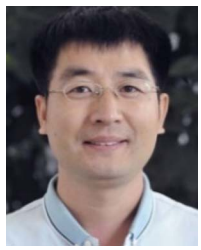

Yong Lu received the Ph.D. degree in signal and information systems from Beihang University, Beijing, China, in 2009. He is currently a Professor with the College of Power and Energy Engineering, Harbin Engineering University, Harbin, China. He has authored or co-authored more than 80 articles and more than 50 inventions. His research interests include wireless power transfer, fully variable valve technology, electro-hydraulic servo systems, and ship power plant automation.

Dr. Lu was the recipient of the National Defense Science and Technology Progress Award in 2011 and the Chinese Society of Internal Combustion Engine Outstanding Paper Award in 2017.

Jiayu Zhou received the B.Eng. and M.S. degrees in electrical engineering from Beijing Jiaotong University, Beijing, China, in 2016 and 2019, and the Ph.D. degree in engineering cybernetics from the Norwegian University of Science and Technology, Trondheim, Norway, in 2023.

Since 2023, he has been a Postdoctoral Research Fellow with City University of Hong Kong, University of Hong Kong, Hong Kong. His research interests include inductive power transfer and power converters for renewable energy system.